iScience

CellPress
OPEN ACCESS

Article

Super-spreading on superamphiphilic micro-organized nanochannel anodic aluminum oxide surfaces for heat dissipation

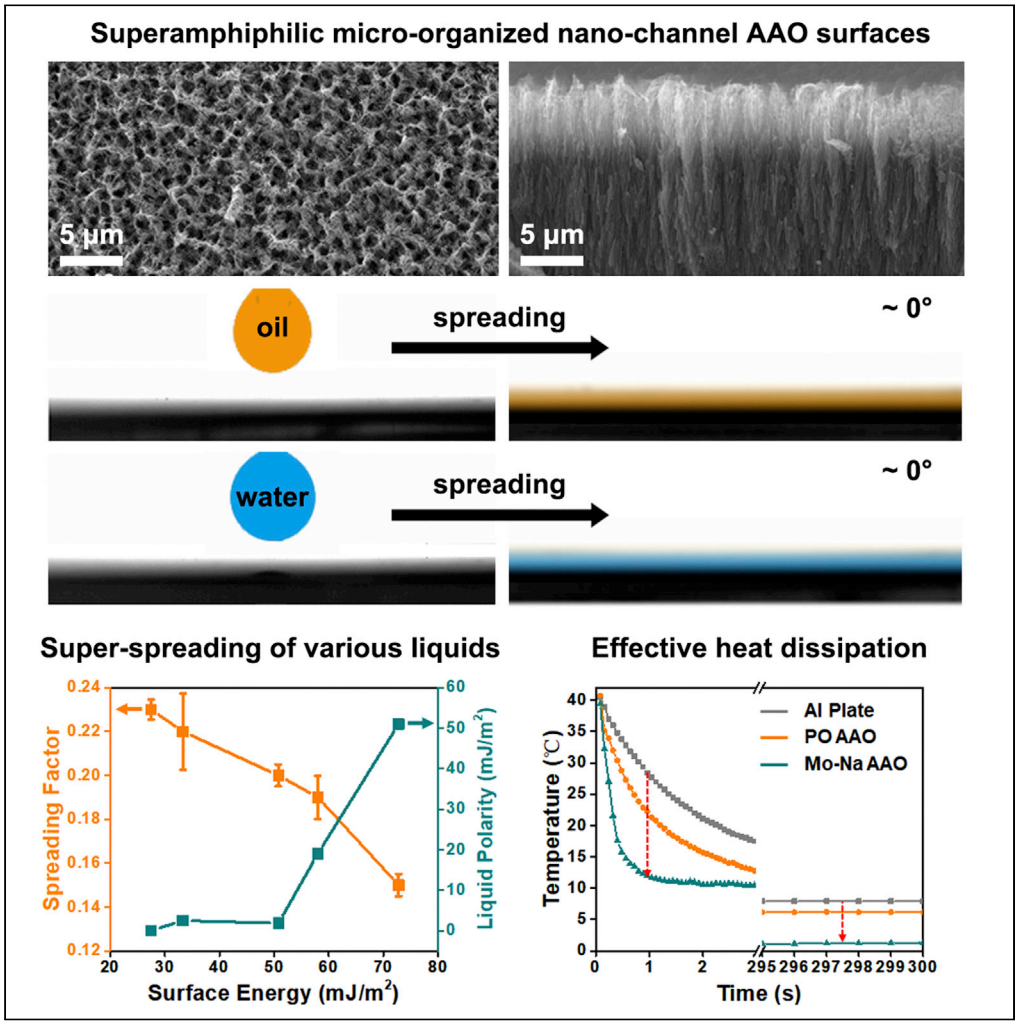

Zhongpeng Zhu, Yupeng Chen, Zhe Xu, ..., Jiajia Zhou, Ye Tian, Lei Jiang

tianyely@iccas.ac.cn (Y.T.)
jianglei@iccas.ac.cn (L.J.)

Highlights

Discovery of micro-organized nano-channel superamphiphilic AAO structures

One-step anodization method to prepared long-lasting superamphiphilic AAO surfaces

Effective heat dissipation property based on the super-spreading behaviors

Zhu et al., iScience *24*, 102334
April 23, 2021
https://doi.org/10.1016/j.isci.2021.102334

iScience

CellPress
OPEN ACCESS

Article

Super-spreading on superamphiphilic micro-organized nanochannel anodic aluminum oxide surfaces for heat dissipation

Zhongpeng Zhu,[1] Yupeng Chen,[1] Zhe Xu,[1] Zhenwei Yu,[1] Xianfeng Luo,[4] Jiajia Zhou,[1] Ye Tian,[2,3,5,*] and Lei Jiang[1,2,3,*]

SUMMARY

Nature-inspired superamphiphilic surfaces have drawn tremendous attention owing to its extreme liquid-loving behaviors. Herein, a micro-organized nanochannel (Mo-Na) superamphiphilic anodic aluminum oxide (AAO) surface with long-lasting superamphiphilic property is prepared by a facile one-step anodization method with controllable temperature change. Analysis of dynamic wetting behaviors on superamphiphilic Mo-Na AAO surfaces for various liquids reveals that the spreading factor is in negative correlation with the surface tension and liquid polarity. Detailed observation of the three-phase contact line shows a micro-scale capillary film on superamphiphilic Mo-Na AAO surfaces, which results from the horizontal component of the capillary force. Taking advantage of the superamphiphilic property, water droplets can spread completely on these Mo-Na AAO surfaces within a short time, which can be applied for efficient heat dissipation. Moreover, the unique AAO surface with Mo-Na structures also offers an effective template for future efforts in AAO-based composite devices.

INTRODUCTION

Nature-inspired surfaces with extreme wettability have been widely studied (Archer et al., 2020; Aussillous and Quere, 2001; Chen et al., 2018). For example, nature-inspired artificial superhydrophobic surfaces are widely applied in various fields including self-cleaning, anti-icing, power generation, catalysis, liquid manipulation, and so forth (Liu et al., 2019; Sun et al., 2019; Tian et al., 2016; Zhu et al., 2021). On the other hand, nature-inspired superamphiphilic surfaces on which both water and oil can spread completely are still in infancy and raise increasing attentions (Miao et al., 2019). Generally, liquid can completely spread on superamphiphilic surfaces with apparent contact angles near 0° (Zhu et al., 2017b). The spreading process can be analyzed with the spreading factor by recording the spreading radius (or contact angle) over time, and the final spreading state can be described with the spreading coefficient by evaluating the total force at the three-phase contact line (Harkins and Feldman, 1922; Tanner, 1979). When the spreading coefficient is positive, the three-phase contact line continues moving forward without pinning. Benefiting from the super-spreading behaviors, thin liquid film covers a large contact area on solid, which can be utilized both in scientific research and industrial applications. For example, thin and uniform functional films can be generated on superamphiphilic surfaces in both organic and inorganic solvents, which presents a facile and low-cost method in device fabrications (Zhao et al., 2020; Zhu et al., 2017a). Besides, taking advantage of the strong interactions between liquid molecules and solid substrates, superamphiphilic surfaces can be used in liquid-infused anti-corrosion, anti-fogging, and self-cleaning for ships and vehicles (Fujishima et al., 2008; Wang et al., 2012; Yao et al., 2013). Moreover, based on the controllable super-spreading behaviors, liquid manipulation can be achieved both in painting and liquid separation (Min et al., 2019; Sun et al., 2020; Wang et al., 2017; Zheng et al., 2018). Previous studies showed that the superamphiphilic surfaces can be obtained based on photocatalytic materials such as TiO_2, PbS/CdS, *etc* (Li et al., 2010; Wang et al., 1997), or various treatment methods such as plasma, surface grafting, spin coating, *etc*. (Bui et al., 2015; Wu et al., 2016; Zheng et al., 2016) However, the low durability and complex fabrication process with limited structures of superamphiphilic surfaces are still main problems. Various approaches were proposed to construct surfaces with extreme wettability, and the *in situ* anodization method to growth oxide layer is found to be a facile one with the advantage of high durability, offering an effective approach to prepare superamphiphilic surfaces (Nakajima et al., 2019; Shahi, 2010; Tang et al., 2006).

[1]Key Laboratory of Bio-inspired Smart Interfacial Science and Technology of Ministry of Education, School of Chemistry, Beihang University, Beijing 100191, P. R. China

[2]Key Laboratory of Bioinspired Smart Interfacial Science, Technical Institute of Physics and Chemistry, Chinese Academy of Sciences, Beijing 100190, P. R. China

[3]University of Chinese Academy of Sciences, Beijing 100049, P. R. China

[4]College of Chemical and Environmental Engineering, Harbin University of Science and Technology, Xuefu Road, No. 52, Harbin 150080, Heilongjiang, PR China

[5]Lead contact

*Correspondence: tianyely@iccas.ac.cn (Y.T.), jianglei@iccas.ac.cn (L.J.)

https://doi.org/10.1016/j.isci.2021.102334

Among various *in situ* growth methods, the anodization process to grow anodic aluminum oxide (AAO) layer with long-range ordered hexagonal structures on aluminum (Al) surfaces is widely used (Li et al., 2018; Wen et al., 2017). Generally, nanoscale ordered AAO surfaces are studied and used as templates to fabricate various nanostructures (Lee and Park, 2014). Improving the interfacial wettability can effectively enhance the application of AAO templates by constructing various structures. For example, three-dimensional interconnected nanoarchitectures are generally prepared with superhydrophilic properties (Dudem et al., 2016; Martin et al., 2014; Ye et al., 2009). But the limited nanoscale structures of AAO surfaces restricted their applications, and hierarchical AAO surfaces with micro-nano composite structures of unique properties drew more and more attention, especially in photovoltaic devices, optics, sensors, and so on (Fan et al., 2009; Lee et al., 2017; Zhang et al., 2017). To fabricate micro-nano hierarchical structures with extreme wettability, several typical methods were reported such as regulating the anodization time (Kang et al., 2015), changing the type and concentration of electrolyte (Kikuchi et al., 2014), laser-assisted solvent spreading (Lv et al., 2015), etc. However, these methods to fabricate hierarchical AAO surfaces are usually complex and time-consuming involve several steps such as heat treatment, polishing, first anodization, second anodization, pore etching, laser treatment, and so forth (Bae et al., 2015). Hence a facile fabrication method to prepare ordered hierarchical AAO surfaces with superamphiphilic property is still a remaining challenge.

In this work, micro-organized nano-channel (Mo-Na) AAO surfaces were prepared by a facile one-step anodization method with controllable temperature change. The as-prepared superamphiphilic Mo-Na AAO surfaces showed super-spreading behaviors with liquid contact angles of near 0° for water and various kinds of organic liquids. Detailed analysis of the spreading factors for various liquids revealed that the spreading speed is inversed correlated to surface tension and liquid polarity. Further observation of the three-phase contact line revealed a micro-scale capillary film on Mo-Na AAO surfaces indicating the spreading coefficient is positive owing to the existence of horizontal capillary forces, which results in the super-spreading behaviors. Besides, the superamphiphilic property of Mo-Na AAO surface can last for more than one month, which demonstrates the long-term stability. Based on the super-spreading behaviors induced by strong capillary forces of three-dimensional interconnected nano-channels, effective evaporation and heat dissipation behaviors were demonstrated on these superamphiphilic Mo-Na AAO surfaces. This work provides a facile method to prepare hierarchical ordered superamphiphilic Mo-Na AAO surfaces which offers an intriguing template platform for replica of functional materials, generation of composite devices, construction of sensors, and so on.

RESULTS AND DISCUSSION

Mo-Na AAO surfaces

AAO surfaces with porous-ordered (PO) structures and Mo-Na hierarchically ordered structures can be obtained by a facile one-step anodization method with controllable temperature change at constant anodization currents based on high purity Al plates, as shown in Figure 1A. Contact angle measurements revealed that the Al plate with a native oxide layer is amphiphilic (23.3 $\pm$ 3.4° for water and 42.6 $\pm$ 3.9° for diiodomethane). Traditionally, hexagonal long-range ordered AAO structures can be obtained at a constant temperature with agitation, as shown in Figure 1B. However, the temperature of electrolyte would increase dramatically without agitation owing to the heat production during anodization. In this study, the electrolyte was cooled down to around 0°C under agitation before the anodization process. Then the anodization process was carried out without agitation at different constant anodization currents (detailed surface structures are shown in Figure S1). In this case, the temperature of the electrolyte would rise along with the anodization process, which resulted in various AAO structures. At a low anodization current, the temperature change of the electrolyte is within 20°C, which resulted in the growth of porous tubular AAO structures. The PO AAO with tubular structures shows a diameter of 237.2 $\pm$ 44.7 nm and amphiphilic property with water and diiodomethane contact angles of 37.5 $\pm$ 3.7° and 60.8 $\pm$ 1.8°, respectively. In contrast, with the continuous increase of the anodization current, Mo-Na AAO surfaces (pore diameter in bulk 177.1 $\pm$ 30.6 nm and pore diameter at surface 0.89 $\pm$ 0.28 μm) gradually formed. It is intriguing to notice that nano-channels were etched to nano-fibers at the surface, which further self-organized into micro-holes. Meanwhile, nano-channels in the bulk formed centrally convergent micro-branches with three-dimensional interconnected structures (Figure 1C). It is worth noting that the temperature change of electrolyte during this process is within 80°C, indicating the violent growth and etching processes of AAO layers. Further measurements revealed that both water and diiodomethane droplets spread completely with contact angles of 0 $\pm$ 0.1°, indicating the Mo-Na AAO surface is superamphiphilic. Besides, taking advantage of the super-

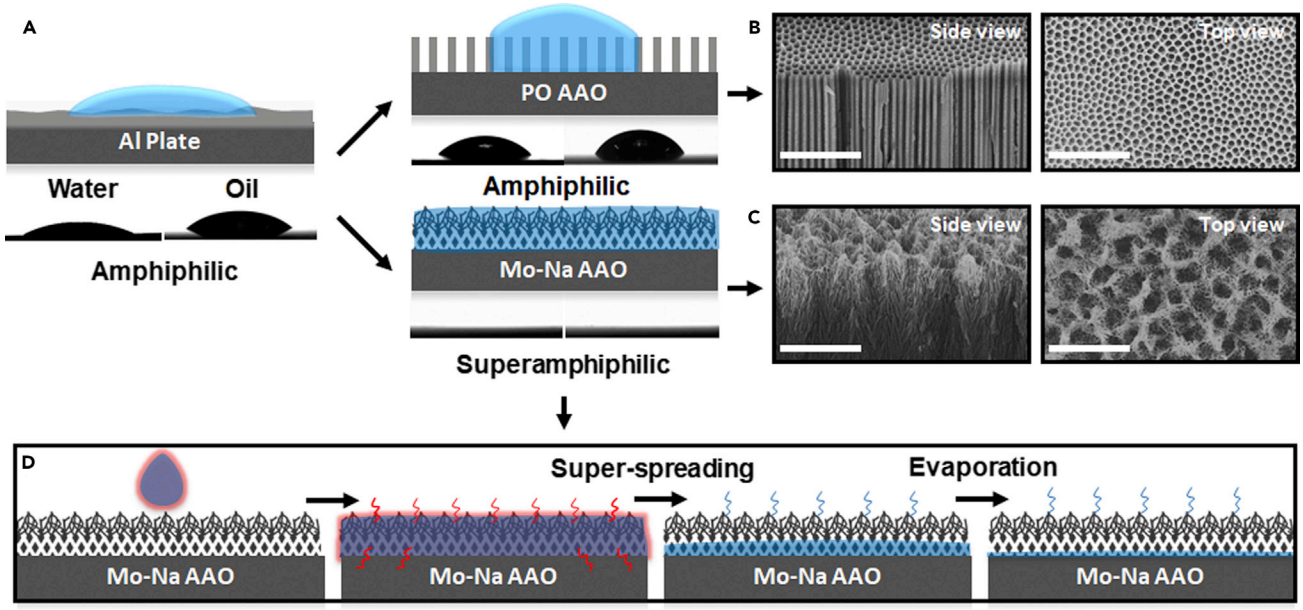

Figure 1. Schematic diagram of aluminum (Al) plate, porous-ordered (PO) and micro-organized nano-channel (Mo-Na) AAO surfaces, as well as the demonstration of heat dissipation process.

(A–C) (A) Amphiphilic Al plates can be anodized to amphiphilic PO AAO surfaces and superamphiphilic Mo-Na AAO surfaces. Scanning electronic microscopy images revealed the tubular structures of PO AAO surfaces (B) and three-dimensional interconnected nano-channels of Mo-Na AAO surfaces (C). (scale bar is 5 μm).

(D) Schematic drawing demonstrates the effective heat dissipation process on Mo-Na AAO surfaces, taking advantage of the evaporation effect owing to the super-spreading behaviors.

spreading behaviors on superamphiphilic Mo-Na AAO surfaces, effective evaporation and heat dissipation can be achieved, as shown in Figure 1D. The heat dissipation process can be divided into two typical processes. One is the super-spreading process, in this case liquid with high temperature can dissipate the heat within a short time, which can be applied in collection and heat dissipation of steam in power stations. The other is the evaporation process resulting from the large super-spreading areas, which can be applied in cooling of substrates for computers and air conditions.

Study of the static and dynamic wettability on Mo-Na AAO surfaces

The static wettability was studied concerning the anodization process and long-term stability. It is known that there are several factors which affect the structure of AAO surfaces during the anodization process, such as electrolyte type, anodization current, anodization time, anodization temperature, electrolyte concentration, *etc.* (Masuda and Fukuda, 1995) In this study, phosphoric acid is used as the electrolyte to achieve fast anodization at high voltage (Lee et al., 2006). To reveal the critical threshold for constructing superamphiphilic Mo-Na AAO surfaces, contact angles of these surfaces with the variation of anodization current and time were studied. As shown in Figure 2A, contact angles of water and diiodomethane decrease with the increase of the anodization current. Interfacial structure observation by scanning electronic microscopy revealed that PO AAO surfaces formed at a constant anodization current lower than 1.5 A. In this stage, the temperature change of the electrolyte is within 20°C and straight tubular nano-channel structures are formed in the AAO layer. When the anodization current is higher than 1.5 A, these surfaces become superamphiphilic with contact angles of both water and diiodomethane reaching 0°. Since the resistance of Al substrate is relatively low in this system, the total resistance measured during the anodization process can be attributed to the growth of non-conducting AAO layers. With the increase of current, the balanced resistance gradually decreases, which means the increase of the anodization current can reduce the thickness of AAO layers (Figure S2A). Besides the anodization current, the influence of anodization time was also studied with a constant anodization current of 2.0 A. As shown in Figure 2B, contact angles of both water and diiodomethane decrease sharply with the increase of anodization time, and eventually both drop to 0 $\pm$ 0.1° when the anodization time exceeds 280 s. By recording the resistance-time curve during the anodization process, it was found that the balanced resistance drops to the lowest point

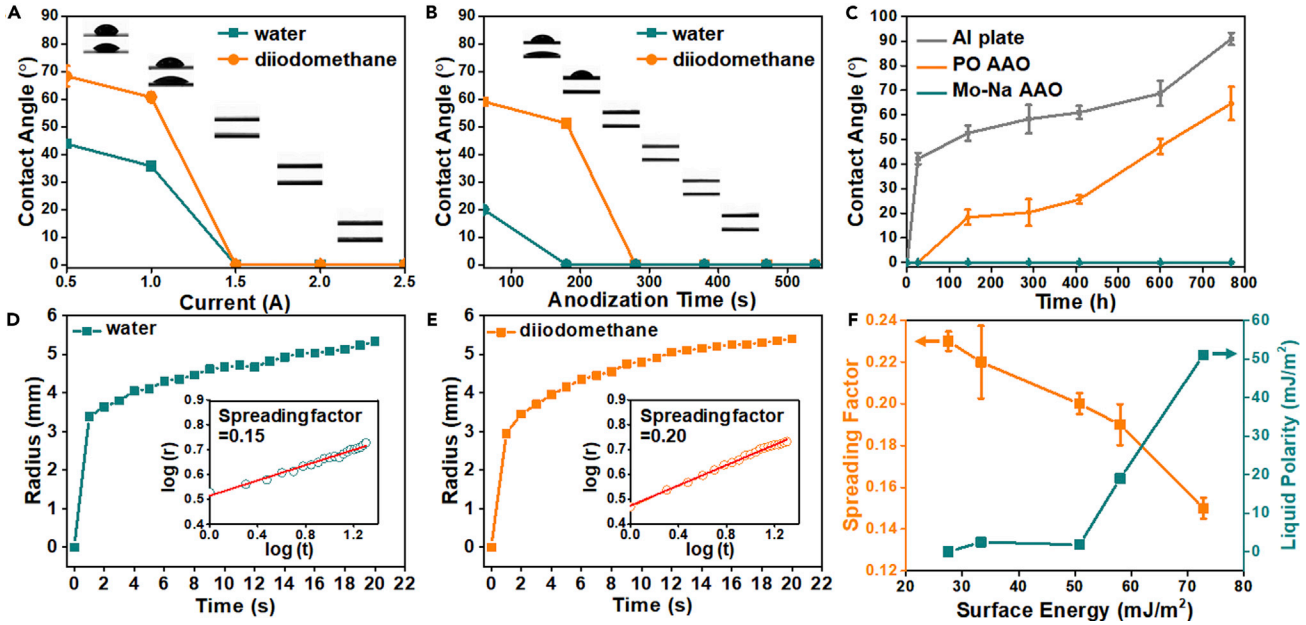

Figure 2. Analysis of the static and dynamic wettability with various liquids on Mo-Na AAO surfaces

(A) Static contact angle measurements reveal that the superamphiphilic Mo-Na AAO surfaces can be obtained with the anodization current higher than 1.5 A.

(B) Contact angle measurements indicated the anodization time needs to exceed 280 s to obtain superamphiphilic AAO surfaces.

(C) Compared with plasma-treated Al plates and PO AAO surfaces, the superamphiphilic Mo-Na AAO surfaces can last for more than one month.

(D and E) Dynamic wetting behaviors were studied by recording the spreading radius over time, and the inset shows the detailed calculation process of spreading factors.

(F) Spreading factors of various liquids are summarized compared with liquid surface tension and polarity, which shows the spreading speed is in negative correlation with the surface tension and liquid polarity.

at the anodization time of around 280 s and then steadily increased, which means the increase of anodization time increases the balanced thickness of AAO layers (Figure S2B). Herein, it is found that the superamphiphilic AAO surface is strongly related to the anodization current and time, which affect the etching speed and the growing rate of AAO layers, respectively. It is inferred that the low resistance may result from the increased etching process induced by the high temperature of electrolyte at high anodization currents. In this case, hairy AAO fibers formed and further self-organized into micro-holes at the surface. Besides, the tubular nano-channels formed connected nano-channels and centrally converged to branched structures in the bulk. When these three-dimensional interconnected nano-channels are formed, the surface shows superamphiphilic property with contact angles of both water and diiodomethane approaching 0°. Compared with the anodization current and time, the concentration of electrolyte showed little effect on the wettability at a constant anodization current of 2.0 A. The long-term stability of AAO surfaces with extreme wettability on different structures were further studied concerning the superhydrophilic property in air, as shown in Figure 2C. Plasma-treated Al plate, PO AAO and Mo-Na AAO surfaces were prepared, water contact angles for all these surfaces were near 0° measured immediately after the treatment. Al plate and PO AAO surfaces lost the superhydrophilic properties in air within one day. And water contact angles continued increasing to 90.9 $\pm$ 2.4° and 64.7 $\pm$ 6.8° for Al plate and PO AAO, respectively. In contrast, water contact angles remained near 0° after more than one month on Mo-Na AAO surfaces, indicating the long-term stability of this surface.

Besides the static wettability of various AAO surfaces, the dynamic wettability of liquids with various surface energies was also investigated on Mo-Na AAO surfaces. By recording the droplet radius during the spreading process, the water and diiodomethane droplets held fast-spreading processes within 2 s and then spread gradually as shown in Figures 2D and 2E. Generally, the spreading process is affected by the balanced forces at the three-phase contact line, including interfacial tension, viscous dissipation, gravity and so forth, which can be further analyzed based on the spreading factor. The spreading factor can be calculated by fitting the time evolution curve of the liquid spreading radius (defined as the dynamic radius of capillary film) recorded by a high-speed camera, and can be analyzed as shown below:

$$R(t) \sim At^n$$

where R is the droplet radius, t is time, A is a front factor depending on the surface tension γ, and the liquid viscosity μ. This power-law scaling only applies to fully wetting fluid with zero contact angle. If the spreading factor n is 1/10, the droplet is spreading on a preexisted precursor films (Liao et al., 2013). While when the fluid spreading into a porous medium, the spreading factor is 1/2 following the standard Lucas-Washburn scaling. In our study, we found the spreading factors of five liquids are between 0.14 and 0.23, which are higher than the power law (1/10) and smaller than the standard Lucas-Washburn scaling (1/2). As shown in Figure 2F, with the increase of the liquid surface tension, namely hexadecane (Figure S3), 1,2-dichloroethane, diiodomethane, formamide and water, the corresponding spreading factors decreased gradually. Further surface energy calculation reveals that the decrease of spreading factors is also inversed correlated to the liquid polarity (Table S1). Fourier transform infrared measurements indicate that there are plenty of polar hydroxyl groups on the AAO surface that can hold a strong interaction with the polar liquids (Figure S4). In this case, the viscous dissipation during the liquid spreading process will increase owing to the polar-polar interaction, and in turn, the corresponding spreading factors decreased.

Characterization of three-phase contact line on AAO surfaces

Macroscopic wettability in air is mainly attributed to the state of the three-phase contact line determined by the balanced forces of solid, liquid and air (Huhtamäki et al., 2018; Snoeijer and Andreotti, 2013). A recent study of *Sarracenia trichome* demonstrated that micro-structures play a critical role in the liquid spreading process (Chen et al., 2018). It was found that the ultrafast water transport process resulted from the hierarchical micro-channels of the trichome, which can be further explained by a two-step transport mechanism. In our study, the ordered micro-structures are observed after the disordered growth of AAO layers during the anodization process, which are self-assembled micro-holes formed by nano-fibers at the surface and centrally convergent micro-branched nano-channels in the bulk. To further reveal the effect of micro-scale surface structures, the state of the three-phase contact line for water droplets on Al plate and AAO surfaces with PO and Mo-Na structures were studied. Detailed observation by laser confocal microscope revealed various states of the three-phase contact line, as shown in Figure 3A. Since water droplets hold a certain shape on Al plate, the three-phase contact line of water droplets pinned in air. Generally, liquids pinned at solid surfaces can be explained by the balanced forces at three-phase contact line of solid/air, liquid/air and liquid/solid, as indicated by the black dot and capillary force ($F_{capillary} = 0$) is not involved (Figure 3B). However, when surface structures are introduced, the forces act at three-phase contact line would change owing to the additional capillary effects. Owing to the tubular structures on PO AAO surfaces, an additional capillary effect is applied on the three-phase contact line of water droplets ($F_{capillary} > 0$). Since these AAO tubes are vertically downward which results in an additional vertical capillary force ($F_V > 0$) and horizontal capillary force (F_H) is negligible, the three-phase contact line of water droplets pins in air (Figure 3C). In this case, the additional $F_{capillary}$ has little effect on the horizontal spreading process as the schematic diagram shown in Figure 3D. In contrast, water droplets on Mo-Na AAO surface continue spreading with a millimeter-scale capillary film (Figure 3E). It is worth noting that the edge of thin capillary films of water droplets showed finger-spreading behaviors indicating strong capillary forces generated by the self-organized nano-fibers at the surface and the three-dimensional interconnected nano-channels in the bulk. As shown in Figure 3F, since the interconnected nano-channels in Mo-Na AAO surfaces are not perpendicular to the surface, the additional $F_{capillary}$ would show both horizontal and vertical components ($F_H > 0$, $F_V > 0$), which results in the continuous spreading of water droplets.

Effective heat dissipation on Mo-Na AAO surfaces

Nowadays, Al is a widely used material in heat dissipative devices owing to its high thermal conductivity. Through increasing the contact area between cooling agent and Al substrate, the heat exchange rate in air condition, supercomputer, power station and so forth can be significantly enhanced. By introducing superamphiphilic Mo-Na AAO surfaces with fast liquid spreading behaviors, it is expected that the effective heat dissipative property can be achieved. Effective evaporation is a prerequisite for effective heat dissipation. As shown in Figure 4A, owing to the super-spreading induced fast evaporation process, water droplet holds an evaporation rate of 1.44 mg/min, which is around 3 times higher than the evaporation rate on Al plate and PO AAO surfaces with 0.53 mg/min and 0.47 mg/min, respectively. Taking advantage of the infrared thermal camera, heat dissipative process is studied by recording the temperature versus time curve for a single water droplet of around 41°C placed on Al plate and AAO surfaces with PO and Mo-Na structures (Figure 4B). Detailed analysis of temperature change is shown in Figure 4C. As a result of the poor

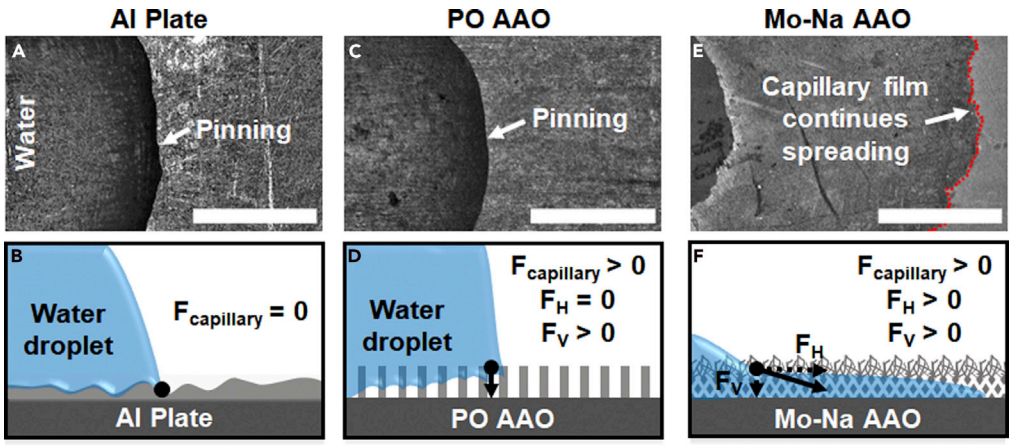

Figure 3. Characterization of three-phase contact line on AAO surfaces with three typical structures

(A) Optical images of the spreading edge for water droplets on Al plates. (scale bar is 1 mm).

(B) Schematic diagram indicates the pinning of the three-phase contact line results from the balanced forces at the three-phase contact line.

(C) Optical images of the spreading edge for water droplets on PO AAO surfaces.

(D) Schematic diagram shows the vertical capillary forces (F_V) assist the pinning of the three-phase contact line.

(E) The three-phase contact line continues spreading on Mo-Na AAO surfaces with a millimeter-scale capillary film.

(F) Detailed schematic diagram of the three-phase contact line on Mo-Na AAO surfaces showing the horizontal capillary forces (F_H) that assist the continuous spreading process.

surface wettability of Al plate and PO AAO surfaces, water droplets deposited on these surfaces held restricted heat exchange areas between liquid and the solid substrate at the surface. In turn, the temperature of water droplets decreased slowly. In contrast, water droplets spread completely on Mo-Na AAO surfaces with large solid-liquid contact areas. In turn, the temperature of water droplets drops to near room temperature (around 10°C) within a short time. Detailed analysis revealed that this phenomenon is not only significantly effective for heat dissipation at the initial stage but also for a relatively long period. At the initial stage within 1 s, the heat dissipative rate of water droplets on Mo-Na AAO surfaces is around 29.35°C/s, while the heat dissipative rates of water droplets on Al plate and PO AAO surfaces are 13.34°C/s and 19.69°C/s, respectively. Hence heat can be transferred to the superamphiphilic Mo-Na AAO surfaces more effectively within a short time. On the other hand, taking advantage of liquid evaporation, the temperature of AAO surfaces with water droplets or water film can both decrease below the room temperature over a relatively long period (around 300 s). In this experiment, the temperature of Mo-Na AAO surface for a relatively long period (7.93°C) is around 6.7°C lower than that of Al plate (1.23°C). Hence, it can be seen the heat dissipative efficiency of Mo-Na AAO surfaces is relatively high both at the initial stage and for a relatively long period than Al plate and PO AAO surfaces.

Conclusion

In summary, superamphiphilic Mo-Na AAO surfaces with long-term stability are reported by a facile one-step anodization method with controllable temperature change. Contact angle measurements combined with resistance curves revealed that the superamphiphilic Mo-Na AAO surfaces formed owing to the balance of growth and etching process in anodization. The superamphiphilic Mo-Na AAO surfaces show long-term stability which can last for more than one month. Further calculation of the spreading factors based on liquids with different surface tension indicates that the liquid spreading speed is inversed correlated to the total surface tension and liquid polarity. Detailed observation of the spreading edge of water droplets reveals that the three-phase contact line continues moving with a millimeter-scale capillary film on superamphiphilic Mo-Na AAO surfaces, which can be attributed to the horizontal capillary forces induced by hierarchical interconnected nano-channels. Taking advantage of the super-spreading property resulted from the interconnected nano-channels of Mo-Na AAO structure, heat dissipation based on effective evaporation is demonstrated, which can be used in desalination and heat dissipative devices. Besides, the superamphiphilic Mo-Na AAO surfaces with ordered structures both in micro- and nano-scale

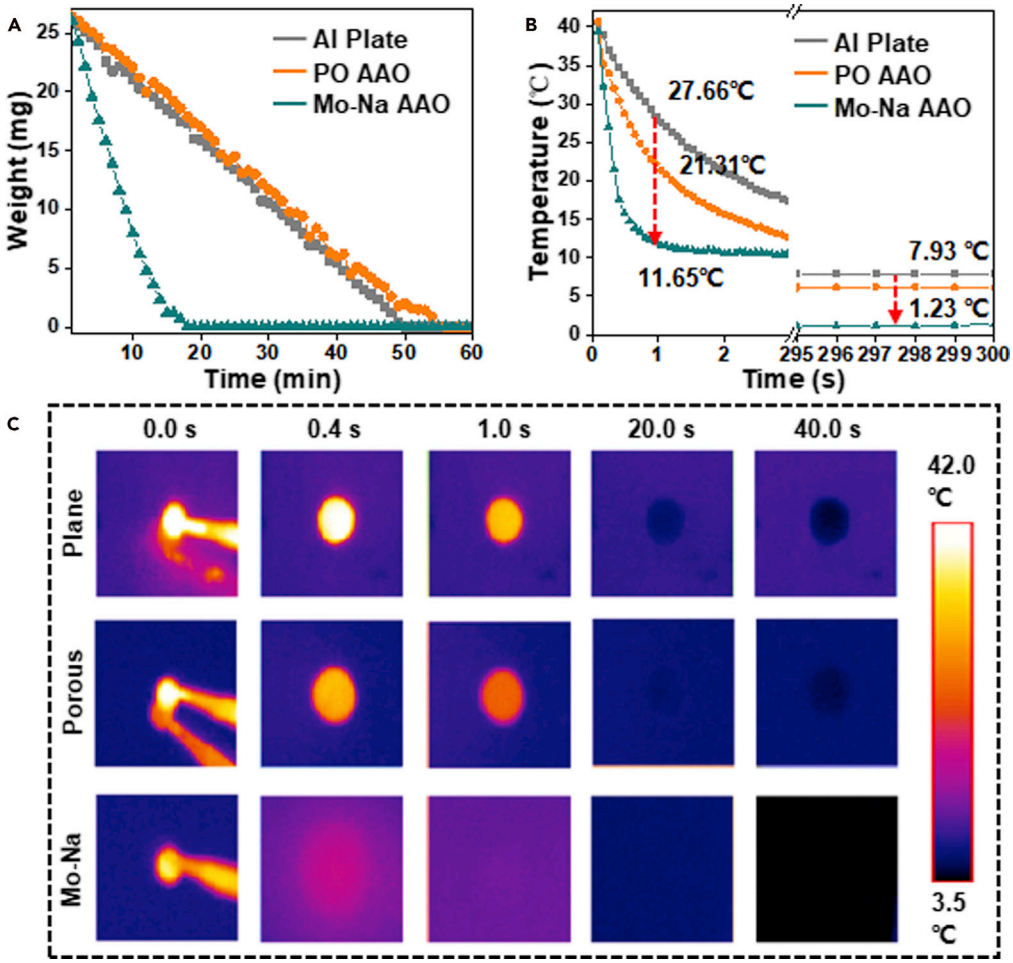

Figure 4. Evaporation and heat dissipation behaviors on three typical surfaces

(A) Evaporation process is evaluated by measuring the weight change of water droplets, indicating the evaporation rate on Mo-Na AAO surfaces is around 3 times higher compared with Al plates and PO AAO surfaces.

(B) The infrared thermal camera reveals the heat dissipation process of a single water droplet with the initial temperature around 41°C on three typical surfaces.

(C) Detailed change of surface temperature reveals that the heat dissipation efficiency on Mo-Na AAO is higher than Al plates and PO AAO surfaces both at the initial stage and for a relatively long period.

may find other applications in AAO-based templates, sensors, organic-inorganic hybrid devices, and so forth.

Limitations of the study

The size of self-assembled micro-holes at the surface and the interconnected nano-channels in the bulk are significant factors for the liquid spreading process. In this work, we discovered the facile single-step method with controllable temperature change to generate these two structures at the same time, however, the micro- and nano-pores are not well adjusted, which is the main limitation of current work.

Resource availability

Lead contact

Further information and requests for resources and reagents should be directed to and will be fulfilled by the lead contact, Ye Tian, (tianyely@iccas.ac.cn.)

Materials availability

This study did not generate any new unique reagent.

Data and code availability

All data used in the study are included in this publication. The present research did not use any new codes.

METHODS

All methods can be found in the accompanying transparent methods supplemental file.

SUPPLEMENTAL INFORMATION

Supplemental information can be found online at https://doi.org/10.1016/j.isci.2021.102334.

ACKNOWLEDGMENTS

This research is supported by the National Research Fund for Fundamental Key Projects of China (2017YFA0204504, 2018YFA0208502), National Natural Science Foundation (21972154, 21988102, 22090052, 22002005, 52003012, 21902006), Frontier Science Key Projects of CAS (ZDBS-LY-SLH022) and Beijing Municipal Science and Technology Commission No. Z181100000441801, and China Postdoctoral Science Foundation (2019M660397, 2019TQ0014).

AUTHOR CONTRIBUTIONS

Z.P.Z. and Y.P.C. contributed equally to this work. Y.T. and L.J. conceived the project. Z.P.Z. and X.F.L. performed the experiments. J.J.Z. helped to analyzed the spreading process. Z.P.Z. wrote the manuscript. Y.P.C., Z.W.Y., and Z.X. helped to improve the manuscript.

DECLARATION OF INTERESTS

The authors declare no conflict of interests.

Received: January 21, 2021
Revised: February 25, 2021
Accepted: March 16, 2021
Published: April 23, 2021

REFERENCES

Archer, R.J., Becher-Nienhaus, B., Dunderdale, G.J., and Hozumi, A. (2020). Recent progress and future directions of multifunctional (super)wetting smooth/structured surfaces and coatings. Adv. Funct. Mater. *30*, 1907772.

Aussillous, P., and Quere, D. (2001). Liquid marbles. Nature *411*, 924–927.

Bae, K., Kang, G., Cho, S.K., Park, W., Kim, K., and Padilla, W.J. (2015). Flexible thin-film black gold membranes with ultrabroadband plasmonic nanofocusing for efficient solar vapour generation. Nat. Commun. *6*, 10103.

Bui, V.-T., Liu, X., Ko, S.H., and Choi, H.-S. (2015). Super-amphiphilic surface of nano silica/polyurethane hybrid coated PET film via a plasma treatment. J. Colloid Interf. Sci. *453*, 209–215.

Chen, H., Ran, T., Gan, Y., Zhou, J., Zhang, Y., Zhang, L., Zhang, D., and Jiang, L. (2018). Ultrafast water harvesting and transport in hierarchical microchannels. Nat. Mater. *17*, 935–942.

Dudem, B., Leem, J.W., and Yu, J.S. (2016). A multifunctional hierarchical nano/micro-structured silicon surface with omnidirectional antireflection and superhydrophilicity via an anodic aluminum oxide etch mask. RSC Adv. *6*, 3764–3773.

Fan, Z., Razavi, H., Do, J.-w., Moriwaki, A., Ergen, O., Chueh, Y.-L., Leu, P.W., Ho, J.C., Takahashi, T., Reichertz, L.A., et al. (2009). Three-dimensional nanopillar-array photovoltaics on low-cost and flexible substrates. Nat. Mater. *8*, 648–653.

Fujishima, A., Zhang, X.T., and Tryk, D.A. (2008). TiO_2 photocatalysis and related surface phenomena. Surf. Sci. Rep. *63*, 515–582.

Harkins, W.D., and Feldman, A. (1922). Films the spreading of liquids and the spreading coefficient. J. Am. Chem. Soc. *44*, 2665–2685.

Huhtamäki, T., Tian, X., Korhonen, J.T., and Ras, R.H.A. (2018). Surface-wetting characterization using contact-angle measurements. Nat. Protoc. *13*, 1521–1538.

Kang, G., Bae, K., Nam, M., Ko, D.-H., Kim, K., and Padilla, W.J. (2015). Broadband and ultrahigh optical haze thin films with self-aggregated alumina nanowire bundles for photovoltaic applications. Energy Environ. Sci. *8*, 2650–2656.

Kikuchi, T., Nishinaga, O., Nakajima, D., Kawashima, J., Natsui, S., Sakaguchi, N., and Suzuki, R.O. (2014). Ultra-high density single nanometer-scale anodic alumina nanofibers fabricated by pyrophosphoric acid anodizing. Sci. Rep. *4*, 7411.

Lee, J., Shin, S., Jiang, Y.H., Jeong, C., Stone, H.A., and Choi, C.H. (2017). Oil-impregnated Nanoporous oxide layer for corrosion protection with self-healing. Adv. Funct. Mater. *27*, 1606040.

Lee, W., Ji, R., Gösele, U., and Nielsch, K. (2006). Fast fabrication of long-range ordered porous alumina membranes by hard anodization. Nat. Mater. *5*, 741–747.

Lee, W., and Park, S.-J. (2014). Porous anodic aluminum oxide: anodization and templated synthesis of functional nanostructures. Chem. Rev. *114*, 7487–7556.

Li, Q.Y., Kako, T., and Ye, J.H. (2010). PbS/CdS nanocrystal-sensitized titanate network films: enhanced photocatalytic activities and super-amphiphilicity. J. Mater. Chem. *20*, 10187–10192.

Li, X., Zhai, T., Gao, P., Cheng, H., Hou, R., Lou, X., and Xia, F. (2018). Role of outer surface probes for regulating ion gating of nanochannels. Nat. Commun. *9*, 40.

Liao, Y.-C., Li, Y.-C., and Wei, H.-H. (2013). Drastic changes in interfacial hydrodynamics due to wall slippage: slip-intensified film thinning, drop spreading, and capillary instability. Phys. Rev. Lett. *111*, 136001.

Liu, Z., Sheng, X., Wang, D., and Feng, X. (2019). Efficient hydrogen peroxide generation utilizing

photocatalytic oxygen reduction at a triphase interface. iScience *17*, 67–73.

Lv, M., Wang, Q., Meng, Q.a., Zhao, T., Liu, H., and Jiang, L. (2015). Self-assembly of alumina nanowires into controllable micro-patterns by laser-assisted solvent spreading: towards superwetting surfaces. Crystengcomm *17*, 540–545.

Martin, J., Martin-Gonzalez, M., Francisco Fernandez, J., and Caballero-Calero, O. (2014). Ordered three-dimensional interconnected nanoarchitectures in anodic porous alumina. Nat. Commun. *5*, 5130.

Masuda, H., and Fukuda, K. (1995). Ordered metal nanohole arrays made by a two-step replication of honeycomb structures of anodic alumina. Science *268*, 1466–1468.

Miao, W.N., Wang, D., Liu, Z., Tang, J., Zhu, Z., Wang, C., Liu, H., Wen, L., Zheng, S., Tian, Y., et al. (2019). Bioinspired self-healing liquid films for ultradurable electronics. ACS Nano *13*, 3225–3231.

Min, L., Zhang, H., Pan, H., Wu, F., Hu, Y., Sheng, Z., Wang, M., Zhang, M., Wang, S., Chen, X., et al. (2019). Controllable liquid-liquid printing with defect-free, corrosion-resistance, unrestricted wetting condition. iScience *19*, 93–100.

Nakajima, D., Kikuchi, T., Yoshioka, T., Matsushima, H., Ueda, M., Suzuki, R.O., and Natsui, S. (2019). A superhydrophilic aluminum surface with fast water evaporation based on anodic alumina bundle structures via anodizing in pyrophosphoric acid. Materials *12*, 3497.

Shahi, S. (2010). Making silicon superhydrophilic. Nat. Photon. *4*, 350.

Snoeijer, J.H., and Andreotti, B. (2013). Moving contact lines: scales, regimes, and dynamical transitions. Annu. Rev. Fluid Mech. *45*, 269–292.

Sun, L., Bian, F., Wang, Y., Wang, Y., Zhang, X., and Zhao, Y. (2020). Bioinspired programmable wettability arrays for droplets manipulation. Proc. Natl. Acad. Sci. U S A *117*, 4527–4532.

Sun, Q., Wang, D., Li, Y., Zhang, J., Ye, S., Cui, J., Chen, L., Wang, Z., Butt, H.-J., Vollmer, D., et al. (2019). Surface charge printing for programmed droplet transport. Nat. Mater. *18*, 936–941.

Tang, K., Wang, X., Yan, W., Yu, J., and Xu, R. (2006). Fabrication of superhydrophilic Cu_2O and CuO membranes. J. Membr. Sci. *286*, 279–284.

Tanner, L. (1979). The spreading of silicone oil drops on horizontal surfaces. J. Phys. D Appl. Phys. *12*, 1473.

Tian, X.L., Verho, T., and Ras, R.H.A. (2016). Moving superhydrophobic surfaces toward real-world applications. Science *352*, 142–143.

Wang, C., Wang, Z., and Zhang, X. (2012). Amphiphilic building blocks for self-assembly: from amphiphiles to supra-amphiphiles. Acc. Chem. Res. *45*, 608–618.

Wang, R., Hashimoto, K., Fujishima, A., Chikuni, M., Kojima, E., Kitamura, A., Shimohigoshi, M., and Watanabe, T. (1997). Light-induced amphiphilic surfaces. Nature *388*, 431–432.

Wang, Y., Di, J.C., Wang, L., Li, X., Wang, N., Wang, B.X., Tian, Y., Jiang, L., and Yu, J.H. (2017). Infused-liquid-switchable porous nanofibrous membranes for multiphase liquid separation. Nat. Commun. *8*, 575.

Wen, L., Xu, R., Mi, Y., and Lei, Y. (2017). Multiple nanostructures based on anodized aluminium oxide templates. Nat. Nanotechnol. *12*, 244–250.

Wu, C.J., Huang, C.J., Jiang, S.Y., Sheng, Y.J., and Tsao, H.K. (2016). Superhydrophilicity and spontaneous spreading on zwitterionic surfaces: carboxybetaine and sulfobetaine. RSC Adv. *6*, 24827–24834.

Yao, X., Hu, Y., Grinthal, A., Wong, T.-S., Mahadevan, L., and Aizenberg, J. (2013). Adaptive fluid-infused porous films with tunable transparency and wettability. Nat. Mater. *12*, 529–534.

Ye, J.M., Yin, Q.M., and Zhou, Y.L. (2009). Superhydrophilicity of anodic aluminum oxide films: from "honeycomb" to "bird's nest. Thin Solid Films *517*, 6012–6015.

Zhang, Q., Kang, J., Xie, Z., Diao, X., Liu, Z., and Zhai, J. (2017). Highly efficient gating of electrically actuated nanochannels for pulsatile drug delivery stemming from a reversible wettability switch. Adv. Mater. *30*, 1703323–n/a.

Zhao, C., Zhang, P., Zhou, J., Qi, S., Yamauchi, Y., Shi, R., Fang, R., Ishida, Y., Wang, S., Tomsia, A.P., et al. (2020). Layered nanocomposites by shear-flow-induced alignment of nanosheets. Nature *582*, 210–215.

Zheng, S., Du, M., Miao, W.N., Wang, D.Y., Zhu, Z.P., Tian, Y., and Jiang, L. (2018). 2D prior spreading inspired from Chinese Xuan papers. Adv. Funct. Mater. *28*, 1800832.

Zheng, S., Wang, D., Tian, Y., and Jiang, L. (2016). Superhydrophilic coating induced temporary conductivity for low-cost coating and patterning of insulating surfaces. Adv. Funct. Mater. *26*, 9017.

Zhu, Z., Yu, Z., Yun, F.F., Pan, D., Tian, Y., Jiang, L., and Wang, X. (2021). Crystal face dependent intrinsic wettability of metal oxide surfaces. Natl. Sci. Rev. *8*, nwaa166.

Zhu, Z.P., Tian, Y., Chen, Y.P., Gu, Z., Wang, S.T., and Jiang, L. (2017a). Superamphiphilic silicon wafer surfaces and applications for uniform polymer film fabrication. Angew. Chem. Int. Ed. *56*, 5720–5724.

Zhu, Z.P., Zheng, S., Peng, S., Zhao, Y., and Tian, Y. (2017b). Superlyophilic interfaces and their applications. Adv. Mater. *29*, 1703120.

iScience, Volume *24*

Supplemental information

Super-spreading on superamphiphilic micro-organized nanochannel anodic aluminum oxide surfaces for heat dissipation

Zhongpeng Zhu, Yupeng Chen, Zhe Xu, Zhenwei Yu, Xianfeng Luo, Jiajia Zhou, Ye Tian, and Lei Jiang

Transparent Methods

Materials: Aluminum plate and graphite were purchased from Beijing Zhongnuoxincai Co., Ltd. Deionized water was prepared by a Milli-Q system (Millipore, USA) and used for these experiments. Phosphorus acid and sodium hydroxide were purchased from Sigma-Aldrich. Acetone, ethanol, formamide and hexadecane were purchased from Beijing Chemical Reagents Co., Ltd. Diiodomethane and 1,2-dichloroethane were purchased from J&K Beijing Co., Ltd. All chemicals are analytical grade and used as received.

Preparation of AAO surfaces: Aluminum plate with purity of 99.999% and surface roughness of 0.104 μm was cut into rectangular pieces of 2.5 × 4.0 cm^2 which are the same size of the counter electrode of graphite. Then, these rectangular pieces were ultrasonic treated in acetone, ethanol, and deionized water for 10 min, respectively. Before the anodization process, the clean aluminum plates were immersed in 1.0 M NaOH for 60 s to remove the native oxide layer. The electrolyte of phosphorus acid is 0.5 M and cooled down to around 0℃ under stirring at 360 rpm. Then the rectangular piece of aluminum was connected to anode and the graphite was connected to cathode with a distance of around 2 cm. The anodization process was carried out in a constant current mode by a DC power supply (IT6724H, China) without stirring, and the temperature increased during the anodization process. Caution: The fabrication process needs to be carried out in a fume hood, because a lot of hydrogen will be produced during the reaction.

Instrumentation and Characterization: The top-surface and cross-section morphologies of AAO surfaces were observed with a scanning electron microscopy (Hitachi S-4800, Japan) operated at 10 kV. The static contact angle measurements in air were performed using an OCA25 apparatus (DataPhysics OCA25, Germany) at room temperature with liquid volume of around 2 μl. The observation of three-phase contact line was performed by laser confocal microscope

(Olympus OLS-4500, Japan) with liquid volume of around 2 μl. The dynamic wetting behaviors were investigated by a high-speed camera (Olympus i-SPEED 3, Japan) with liquid volume of 1 μl on the AAO surfaces. The weight lose was measured by analytical balance (MS20-DU, Mettler Toledo) with 30 μl water on AAO surfaces with different structures. The heat dissipation process was recorded by an infrared thermal camera (FLIR A615, USA) with a water droplet of 10 μl in ambient conditions (10 ℃, humidity 17%RH).

Supplemental Figures

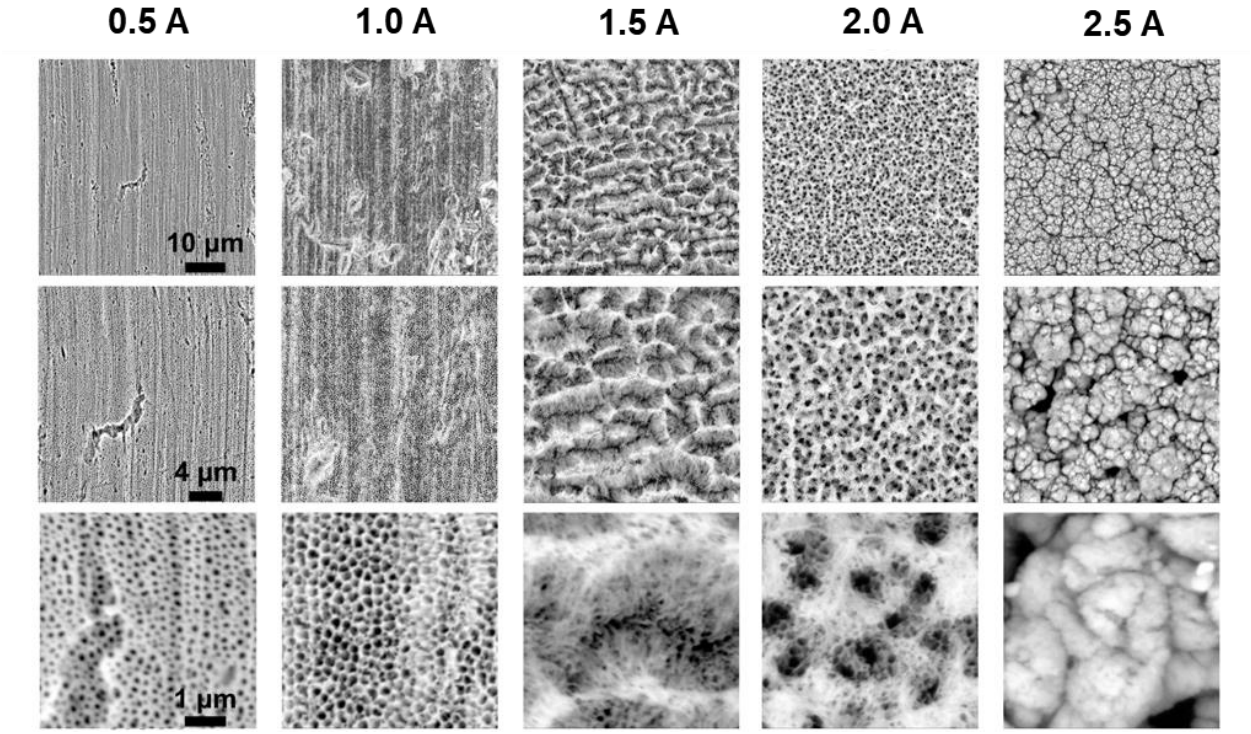

Figure S1. Interfacial structures of AAO surfaces at different anodization current. The etching process is enhanced gradually with the increase of the anodization current, and it is intriguing to find that the disordered nano-fibers can self-organized into micro-holes at the surface when the anodization current reaches 2.0 A. Related to Figure 1.

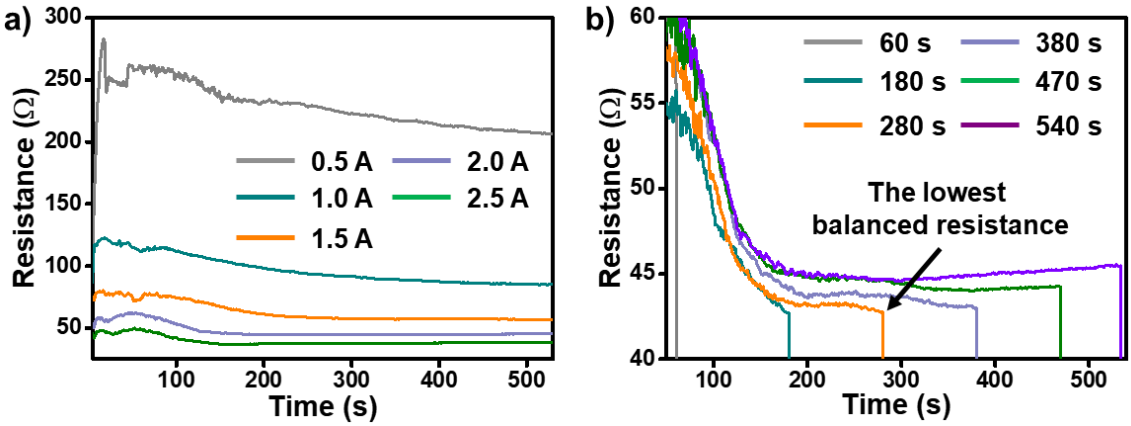

Figure S2. Resistance versus time curve at various anodization current and anodization time. (a) Variation of resistance along time change at different anodization current indicating the increasing of anodization current will reduce the thickness of aluminum oxide layer. (b) Resistance versus time curve at a constant current of 2.0 A indicating the increasing of anodization time will increase the thickness of aluminum oxide layer. Related to Figure 2.

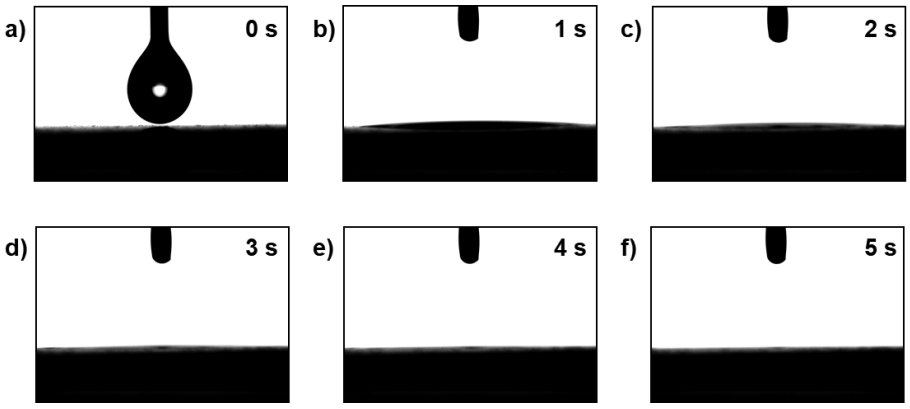

Figure S3. **The contact angle changes of hexadecane over time on SAPL Mo-Na AAO surfaces.** (a-f) Contact angle images of each state captured at the interval of 1 s. Related to Figure 2.

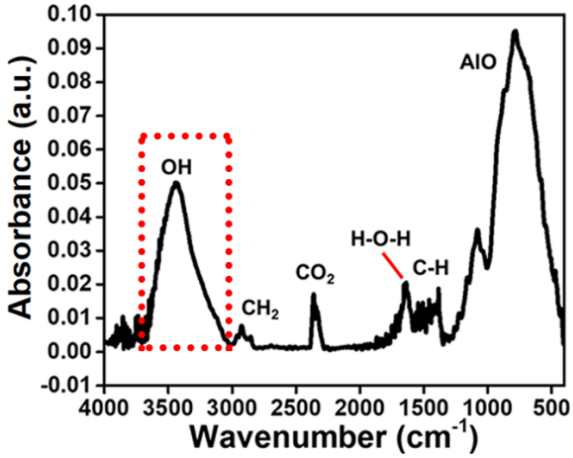

Figure S4. Fourier transform infrared measurements of Mo-Na AAO surface in air. Fourier transform infrared measurements indicate that there are mainly polar groups of hydroxyl, metal-oxygen groups and nonpolar groups of hydrocarbons on the surface. Related to Figure 2.

Liquid	Total surface energy/mJ m^{-2}	Polar surface energy/mJ m^{-2}	Dispersive surface energy/mJ m^{-2}
water	72.8	51	21.8
formamide	58	19	39
diiodomethane	50.8	1.8	49
1,2-dichloroethane	33.3	2.5	30.8
hexadecane	27.5	0	27.5

Supplementary Table 1. **Total surface tension, polar and dispersive components of various liquids. Related to Figure 2.**